

Analysis and interpretation of the Cramér-Rao lower-bound in astrometry: One dimensional case

Rene A. Mendez

Departamento de Astronomía, Facultad de Ciencias Físicas y Matemáticas,
Universidad de Chile, Casilla 36-D, Santiago, Chile

`rmendez@u.uchile.cl`

and

Jorge F. Silva and Rodrigo Lobos

Departamento de Ingeniería Eléctrica, Facultad de Ciencias Físicas y Matemáticas,
Universidad de Chile, Beauchef 850, Santiago, Chile

`josilva, rlobos@ing.uchile.cl`

Received _____; accepted _____

Accepted by PASP

ABSTRACT

In this paper we explore the maximum precision attainable in the location of a point source imaged by a pixel array detector in the presence of a background, as a function of the detector properties. For this we use a well-known result from parametric estimation theory, the so-called Cramér-Rao lower bound. We develop the expressions in the 1-dimensional case of a linear array detector in which the only unknown parameter is the source position. If the object is oversampled by the detector, analytical expressions can be obtained for the Cramér-Rao limit that can be readily used to estimate the limiting precision of an imaging system, and which are very useful for experimental (detector) design, observational planning, or performance estimation of data analysis software: In particular, we demonstrate that for background-dominated sources, the maximum astrometric precision goes as B/F^2 , where B is the background in one pixel, and F is the total flux of the source, while when the background is negligible, this precision goes as F^{-1} . We also explore the dependency of the astrometric precision on: (1) the size of the source (as imaged by the detector), (2) the pixel detector size, and (3) the effect of source de-centering. Putting these results into context, the theoretical Cramér-Rao lower bound is compared to both ground- as well as spaced-based astrometric results, indicating that current techniques approach this limit very closely. It is furthermore demonstrated that practical astrometric estimators like maximum likelihood or least-squares techniques can not formally reach the Cramér-Rao bound, but that they approach this limit in the 1-dimensional case very tightly, for a wide range of S/N of the source. Our results indicate that we have found in the Cramér-Rao lower variance bound a very powerful astrometric “benchmark” estimator concerning the maximum expected positional precision for a point source, given a prescription for the source,

the background, the detector characteristics, and the detection process.

Subject headings: Data Analysis and Techniques, Astronomical Techniques, Stars

1. Introduction

Astrometry relies on the precise determination of the relative location of, usually, point sources. The estimation of the precision with which these measurements can be done, both from an empirical, as well as from a theoretical point of view, has been the subject of various papers. Seminal work, as applied to stellar images recorded on photographic plates, are those of van Altena & Auer (1975) and Auer and van Altena (1978), with further refinements by Lee and van Altena (1983), in which statistical estimations for the precision of the position of stellar images were compared to the results from the actual fitting of stellar profiles measured using microdensitometer scans, through a classical least squares minimization technique assuming a Gaussian noise on the measured intensities.

Nowadays, discrete digital detectors, such as Charged Coupled Devices (CCDs, Howell (2006)), being highly efficient area detectors, are widely used in astronomy for photometric, astrometric and spectroscopic observations (Mackay (1986), for the specific use of CCDs in astrometry see e.g. Monet (1992), Lindegren (2005), and Howell (2013)). This prompted King (1983) to carry out a similar analysis for CCDs, specifically for HST data, starting also from the assumption that a least squares minimization approach provides the best estimation of the relevant parameters.

The studies by Lee and van Altena (1983) and King (1983) (see also Stone (1989)) provide estimates of the statistical uncertainties of the fitted parameters, given a noise model for the data. However, a related question, less often addressed, is what would be the *maximum attainable precision* with which one could expect to estimate the astrometric position of a source, given a prescription of the detection process. This question constitutes a central aspect to astrometric work. For example, in situations, when the detector nearly critically samples the light distribution for point sources rendered by the telescope optics

(case, e.g., of the HST-WFPC imager¹), the question may arise on how well in principle the flux and the position of a point source located on some unknown background may be jointly estimated. The answer may be needed in instrumental design, for planning observation campaigns, or for checking the quality of data analysis algorithms.

In this paper, we concentrate, precisely, on deriving a lower bound to the expected astrometric error for the position of a source in one dimension (hereafter referred to as 1-D), as specified by the variance of the position itself, for the kind of data expected from astronomical CCD-observations. Some seminal work in this area, using the so-called Cramér-Rao bound (Rao (1945), Cramér (1946)), has been presented by Lindegren (1978), Jakobsen et al. (1992), Zaccheo et al. (1995), Adorf (1996), Lindegren (1997) and Bastian (2004). More recently, Lindegren (2010) has published a review paper exploring the astrometric bounds, using some of the Cramér-Rao prescriptions, but focusing mostly on space-based near-diffraction limited imaging. A particularly relevant and inspirational early work on the subject is that contained in Winick (1986) which was focused, however, on read-out noise limited devices and applications. We use Winick’s paper as a starting point of our discussion, expanding it to sky-background limited astronomical observations, and develop it further to explore the general Cramér-Rao bound for astrometry in the 1-D case. We also elaborate on some useful approximations that explicitly expose the dependency of the expected minimum astrometric uncertainty as a function of the parameters characterizing the source and the detector. Some interesting open astrophysical problems that require high-accuracy astrometric measurements have been recently described in the book by van Altena (2013). One may use the maximum expected accuracy estimates developed in this paper to determine whether or not a particular astrophysical problem

¹Instrument handbook available at http://www.stsci.edu/hst/wfpc2/documents/handbook/IHB_17.htm last accessed on December 2012.

- and its associated accuracy requirements - may or may not be tackled with certain instrumental set-up and observing conditions.

2. Preliminaries

To give a formal context, in this section we introduce the basic setting of parameter estimation, as well as some related concepts and definitions, that will be used throughout the paper.

2.1. Parameter estimation and the Cramér-Rao minimum variance bound

The parameter estimation problem at hand can be presented in one-dimension, in general terms, as follows: Let us consider a collection of I_i (with $i = 1..n$) independent and identically distributed realizations of a random variable. In this setting, it will be assumed that the $\{I_i : i = 1, \dots, n\}$ measurements follow an underlying probability (density - if continuous, or mass - if countable) function, denoted by f_θ , which depends upon a certain target (unknown) parameter θ . Then, the parameter estimation problem reduces to find a prescription (or statistics) such that the function $\hat{\theta}(I_1, \dots, I_n)$ is a good approximation of the underlying parameter θ that generated the data.

A standard criterion adopted in statistics to estimate θ is to consider the rule of minimum variance (denoted by Var), given by:

$$\begin{aligned} \hat{\theta}() &\equiv \arg \min_{\hat{\theta}} Var(\hat{\theta}(I_1, \dots, I_n)) \\ &= \arg \min_{\hat{\theta}} \mathbb{E}_{I_1, \dots, I_n \sim f_\theta^n} \left(\hat{\theta}(I_1, \dots, I_n) - \theta \right)^2 \end{aligned} \tag{1}$$

where \mathbb{E} is the expectation value of the argument and “arg min” represents the argument that minimizes the expression. Note that in the last equality we have assumed that $\hat{\theta}()$ is an unbiased estimator of the parameter (i.e., that $\mathbb{E}(\hat{\theta}) = \theta$), so that under this rule we are implicitly minimizing the mean square error of the estimate with respect to the hidden true parameter θ .

Unfortunately, the general solution of equation (1) is intractable, as in principle it requires the knowledge of θ , which is the essence of the inference problem. However, there are performance bounds that characterize how far can we be from the theoretical solution in equation (1), and even scenarios where the optimal solution can be achieved in a closed-form. One of the most significant results in this field is the Cramér-Rao minimum variance bound (Rao (1945), Cramér (1946)) explained below.

Let $\hat{\theta}()$ be an unbiased estimator of θ . If we define the function $L(I_1, \dots, I_n; \theta)$ as the likelihood of the observation given the model parameter θ , and we have n independent random variables I_i driven by the probability function f_θ , then the Cramér-Rao bound states that:

$$\text{Var}(\hat{\theta}(I_1, \dots, I_n)) \equiv \mathbb{E}_{I_1, \dots, I_n \sim f_\theta^n} \left(\hat{\theta}(I_1, \dots, I_n) - \theta \right)^2 \geq \frac{1}{\mathcal{I}_\theta(n)} \quad (2)$$

provided that we satisfy the constraint:

$$\mathbb{E}_{I_1, \dots, I_n \sim f_\theta^n} \left(\frac{d}{d\theta} \ln L(I_1, \dots, I_n; \theta) \right) = 0 \quad (3)$$

and where:

$$\mathcal{I}_\theta(n) \equiv \mathbb{E}_{I_1, \dots, I_n \sim f_\theta^n} \left(\left(\frac{d}{d\theta} \ln L(I_1, \dots, I_n; \theta) \right)^2 \right) \quad (4)$$

is called the *Fisher information* of the data about θ .

A powerful corollary of this result is that the minimum variance of any unbiased estimator that satisfies equation (3) is always going to be greater than the pre-specified quantity given by equation (2).

Generally, this bound is not attained for the minimum variance estimator of θ , however there exists a necessary and sufficient condition that guarantees the existence of an estimate achieving the Cramér-Rao bound, $\mathcal{I}_\theta(n)^{-1}$. More precisely, if we can write (see, e.g., Stuart, et al. (2004, pp. 12)):

$$\frac{d \ln L(I_1, \dots, I_n; \theta)}{d\theta} = A(\theta) \cdot (\hat{\theta}(I_1, \dots, I_n) - \theta) \quad (5)$$

then, it is certain that $Var(\hat{\theta}(I_1, \dots, I_n)) = 1/\mathcal{I}_\theta(n)$, as long as $A(\theta)$ is a function *exclusively* of the parameter θ (and, in particular it does not depend on the observables, I_i)². However, we must keep in mind that, unless the condition in equation (5) is satisfied, the minimum variance solution from equation (1) will have, in general, a variance strictly greater than $\mathcal{I}_\theta(n)^{-1}$. This important result will be further used in Section 5.

2.2. Position estimation: Astrometry

The position estimation in astrometry is a slight variation of the classical parameter estimation problem introduced in Section 2.1. In this paper we focus on the 1-D version, as it is more easily tractable from the numerical and analytical point of view, while capturing all the key elements of the problem. The extension to the 2-D case will be dealt with in a forthcoming paper. However, as we shall see (see Sections 4.1.5 and 5), it is expected that

²Furthermore, in this scenario, it can be easily shown that $A(\theta) = \mathcal{I}_\theta(n)$.

some generalizations are possible from our 1-D results which are likely to be approximately valid on the 2-D scenario in some cases.

In the 1-D case we have an array detector with n pixels, in which we measure the fluxes $\{I_i\}$ per pixel. We will assume that the total *expected* (as opposed to measured) flux at each pixel on the detector, given by a function $\lambda_i(x_c)$, will explicitly depend on the location of the source on the array, denoted by x_c , which is the parameter we want to determine (equivalent to the unknown parameter θ of Section 2.1). Of course, this flux is not measured directly, because the actual observations, I_i , are subject to noise. However, on photon counting devices, such as CCDs, the measured flux follow a Poisson noise distribution, i.e., the I_i are random variables driven by a Poisson distribution (this determines the probability mass function f_θ introduced in Section 2), with expectation value given by $\lambda_i(x_c)$. At this point, we note an important difference in approach to that adopted in the work by Lee and van Altena (1983), in which they have assumed a Gaussian noise per pixel, valid for an analog detector, such as photographic plates. As we shall see, when the noise is Gaussian, a maximum likelihood parameter determination reduces to least squares, which is what they indeed adopted. Note however that King (1983) also adopted a least squares minimization, although for CCDs the noise is not Gaussian, and therefore a maximum likelihood solution *is not* equivalent to a least squares minimization (see Section 5).

In order to estimate the Cramér-Rao bound in this situation, we first need to verify that our likelihood function satisfies equation (3). The likelihood function of the 1-D array observations will be given by:

$$L(I_1, \dots, I_n; x_c) = f_{\lambda_1(x_c)}(I_1) \cdot f_{\lambda_2(x_c)}(I_2) \cdots f_{\lambda_n(x_c)}(I_n) \quad (6)$$

where $f_\lambda(I) = \frac{e^{-\lambda} \lambda^I}{I!}$, since the I_i follow a Poisson mass function distribution with

mean $\lambda_i(x_c)$ ³. Then, we see that:

$$\frac{d \ln L(I_1, \dots, I_n; x_c)}{dx_c} = \frac{d}{dx_c} \left(\sum_{i=1}^n (I_i \cdot \ln \lambda_i(x_c) - \lambda_i(x_c) - \ln I_i!) \right) \quad (7)$$

$$= \sum_{i=1}^n I_i \cdot \frac{1}{\lambda_i(x_c)} \cdot \frac{d\lambda_i(x_c)}{dx_c} - \sum_{i=1}^n \frac{d\lambda_i(x_c)}{dx_c} \quad (8)$$

and, we indeed verify that $\mathbb{E}_{I_1, \dots, I_n} \left(\frac{d \ln L(I_1, \dots, I_n; x_c)}{dx_c} \right) = 0$ because $\mathbb{E}(I_i) = \lambda_i(x_c)$. Hence, we can apply equations (2) and (4) to obtain the following result:

$$\text{Var}(\hat{x}_c(I_1, \dots, I_n)) \geq \frac{1}{\mathcal{I}_{x_c}(n)} = \frac{1}{\sum_{i=1}^n \frac{\left(\frac{d\lambda_i(x_c)}{dx_c} \right)^2}{\lambda_i(x_c)}} \quad (9)$$

For completeness, the derivation of the Fisher information about x_c , $\mathcal{I}_{x_c}(n)$, is presented in Appendix A.

In the following section, we provide a detailed analysis of this expression and its practical implications on astrometry.

3. The astrometric Cramér-Rao minimum variance bound in 1-D

In very general terms, the observed fluxes $\{I_i\}$ will have contributions from the source itself, as well as from a background. Correspondingly, the expected flux (in one pixel) from the source (which explicitly depends on x_c) will be characterized by a function $\tilde{F}_i(x_c)$,

³Note that this estimation setting is different from the classical setting of Section 2.1, since we have random independent, although not identically distributed, samples. Nevertheless, it is simple to prove that equations (2) to (4) still hold under this more general setting.

representing the flux (in photo- e^- on the detector) at pixel i , whereas the expected generic background will be denoted by \tilde{B}_i , representing the total (integrated) background (also in units of e^-) at pixel i , and which includes contributions from the detector (read-out noise and dark-current, if any), and the sky background. We will assume that \tilde{B}_i does not depend on x_c . The total expected flux will thus be given by $\lambda_i(x_c) = \tilde{F}_i(x_c) + \tilde{B}_i$. If we replace this expression for $\lambda_i(x_c)$ into equation (9), we see that:

$$\text{Var}(\hat{x}_c) \geq \sigma_{\text{CR}}^2 = \frac{1}{\sum_{i=1}^n \frac{\left(\frac{d\tilde{F}_i}{dx_c}(x_c)\right)^2}{\left(\tilde{F}_i(x_c) + \tilde{B}_i\right)}} \quad (10)$$

At this point, it is convenient to define a dimensionless, normalized, function $g_i(x_c)$ such that $\tilde{F}_i(x_c) = \tilde{F} \cdot g_i(x_c)$, where \tilde{F} is the total flux of the object (which is invariant to the actual value of x_c). In this case, the RHS of equation (10) can be written as:

$$\sigma_{\text{CR}}^2 = \frac{1}{\sum_{i=1}^n \frac{\left(\tilde{F} \frac{dg_i}{dx_c}(x_c)\right)^2}{\left(\tilde{F} g_i(x_c) + \tilde{B}_i\right)}} \quad (11)$$

Note that this expression is similar to the Cramér-Rao bound derived by Winick (1986) (his equation (35)).

The function $g_i(x_c)$ is determined by the *Point Spread Function* (PSF), which describes the distribution of (source) flux on the detector or, equivalently, the image profile across pixels (represented by the function $\Phi(x)$), integrated over pixel i (of width Δx) of the array, i.e.:

$$g_i(x_c) = \int_{x_i - \frac{\Delta x}{2}}^{x_i + \frac{\Delta x}{2}} \Phi(x) dx \quad (12)$$

Note that the PSF function $\Phi(x)$ is also normalized, i.e.,

$$\int_{-\infty}^{+\infty} \Phi(x) dx = 1 \quad (13)$$

As long as the array length samples a significant fraction of the PSF, we can indeed identify \tilde{F} as the total flux of the star, since:

$$\sum_{i=1}^n \tilde{F}_i = \tilde{F} \sum_{i=1}^n g_i(x_c) = \tilde{F} \sum_{i=1}^n \int_{x_i - \frac{\Delta x}{2}}^{x_i + \frac{\Delta x}{2}} \Phi(x) dx \approx \tilde{F} \int_{-\infty}^{+\infty} \Phi(x) dx = \tilde{F} \quad (14)$$

For practical purposes, since the detector array length greatly exceeds the PSF extent, this means that the source must not be too close to the array boundaries for this equation to be valid.

3.1. Interpretation of the structure of the Cramér-Rao bound

An equivalent to equation (10) in 2-D has been presented, in a slightly different manner, by Lee and van Altena (1983) in the context of the expected astrometric accuracy on photographic plates (their equation (9)). Indeed, it is easy to see that their $\Delta_{ij}^2 \equiv \tilde{F}_{ij}(x_c, y_c) + \tilde{B}_{ij} \equiv \sigma_{\tilde{F}_{ij}}^2 + \sigma_{\tilde{B}_{ij}}^2$, where we have assumed that both, the source and the background, follow Poisson noise (in the case of CCD detectors this is valid when the fluxes are measured in photo-e⁻), and where $\sigma_{\tilde{F}_{ij}}^2$ and $\sigma_{\tilde{B}_{ij}}^2$ are the variances in the source and the background, respectively, at pixel i, j . We emphasize however that their equation (9) has been derived in the case of a (weighted) least squares solution (their equation (5)). This equation is valid for an analog detector, such as photographic plates, where the photographic densities in each pixel are assumed to follow Gaussian noise (see equation (4) in Lee and van Altena (1983)). However, as it will be demonstrated in Section 5), in the

case of digital detectors, where the noise follows a Poisson distribution, no parameter estimator can formally reach the Cramér-Rao bound.

We note that, for Poisson noise, the standard deviation of the signal is the square root of the signal and, thus, the variance is the signal itself. Thus, the interpretation of the term $\tilde{F}_i(x_c) + \tilde{B}_i$ in equation (10) as the *variance* of the counts (in e^-) is important, as indicated in what follows. It is often more convenient for evaluation purposes to express \tilde{F} and \tilde{B} in terms of “counts” on the detector (from now on referred to as “ADUs” - Analog to Digital Units), rather than in e^- , by introducing the so-called (inverse-)gain of the detector G in units of e^-/ADU (see, e.g., Gilliland (1992)). In this case, the source and background fluxes, \tilde{F} and \tilde{B} , are given by $G \cdot F$ and by $G \cdot B$ respectively, where F and B are in units of ADU. On the other hand if $\sigma_{\tilde{F}_i}$ is the rms deviation at pixel i (in e^-) and σ_{F_i} is the equivalent quantity in units of ADUs, then it is true that $\sigma_{\tilde{F}_i} = G \cdot \sigma_{F_i}$, and similarly for the rms deviation on the background. By replacing these unit conversions into either equation (10) or (11) we see that we can express those equations with the source and the background measured in units of either e^- or ADUs, in the sense that:

$$\sigma_{\text{CR}}^2 = \frac{1}{\sum_{i=1}^n \frac{\left(\frac{d\tilde{F}_i}{dx_c}(x_c)\right)^2}{\left(\sigma_{\tilde{F}_i}^2 + \sigma_{\tilde{B}_i}^2\right)}} \quad (15)$$

$$= \frac{1}{\sum_{i=1}^n \frac{\left(\frac{dF_i}{dx_c}(x_c)\right)^2}{\left(\sigma_{F_i}^2 + \sigma_{B_i}^2\right)}} \quad (16)$$

To evaluate the Cramér-Rao bound if we have empirical measurements of *fluxes and variances* on a detector (ADUs), it would obviously be more convenient to use equation (16). However, when performing numerical experiments for a given detector set-up (as done in this paper, Section 5.3), where we only specify flux levels for the source and the background,

and where we *calculate* the variances associated to them, we would instead need to use equation (15) (see also equation (21)). This is because we know that if the flux is in expressed e^- , then the variances are equal to the flux (but this is not the case if the flux is measured in ADUs). We further note that equations (15) or (16) suggest that the Cramér-Rao bound represents a mean “uncertainty over the derivate of the signal”, since:

$$\sigma_{\text{CR}}^2 = \frac{1}{\sum_{i=1}^n \left(\frac{d\tilde{F}_i(x_c)}{\sigma_{\lambda_i}} \right)^2} = \left\langle \left(\frac{\sigma_{\lambda}}{\left(\frac{d\tilde{F}}{dx_c} \right)} \right)^2 \right\rangle \quad (17)$$

where the $\langle \rangle$ stands for a classical type of harmonic mean over the pixels, and where $\sigma_{\lambda_i}^2 = \sigma_{\tilde{F}_i}^2 + \sigma_{B_i}^2$. This provides an interesting connection with what will be presented in Section 5.3: We note that if we have a function of one variable, $y = f(x)$, then⁴ $\sigma_y^2 \simeq \left(\frac{df}{dx} \right)^2 \cdot \sigma_x^2$. If we have n independent measurements, indicated by (x_i, y_i) , each with uncertainty $(\sigma_{x_i}, \sigma_{y_i})$ we know from the propagation of errors in a least squares sense that the minimum variance for the weighted mean \bar{x} would be given by $\sigma_{\bar{x}}^2 = \frac{1}{\sum_{i=1}^n \frac{1}{\sigma_{x_i}^2}} = \frac{1}{\sum_{i=1}^n \left(\frac{\left(\frac{df_i}{dx} \right)}{\sigma_{y_i}} \right)^2}$ (see, e.g., Meyer (1992), Chapter 10), which is equivalent to the Cramér-Rao bound if we identify $f_i = \lambda_i$ and, since the errors follow a Poisson distribution, then $\sigma_{y_i}^2 = \lambda_i$. We emphasize that this analogy is valid only in the 1-D case (otherwise we would need to include the partial derivatives of f , and the variances in all the parameters). Indeed, as we shall see in Section 5, the least squares does not reach, in general, the Cramér-Rao lower bound.

An interesting aspect of equations (10) or (11) is that the positional uncertainty is

⁴Using a Taylor expansion around a point and assuming that f is sufficiently regular or smooth around that point.

going to be dominated by the region near the center of the PSF, where its derivative is steeper. Including regions far from the central core of the PSF, where $\frac{d\tilde{F}_i}{dx_c}(x_c) \sim 0$, will not contribute to a decrease in the uncertainty and, instead, will only deteriorate the overall S/N of the source by incrementally adding more noise than signal (see the paragraph following equation (28)).

3.2. The Cramér-Rao bound for a Gaussian source

It is evident that very little progress can be made in the estimation of the Cramér-Rao bound from equation (11), unless we specify a shape for the PSF. Various analytical forms have been proposed for the PSF of a point source as imaged by ground-based (King 1971) and space-based detectors (King 1983) (but, see also Bendinelli et al. (1988)). Without losing too much generality, in this study we will adopt a Gaussian function which seems to be a good representation of the PSF, at least from the stand-point of astrometric accuracy on ground-based data (Méndez et al. (2010)), and which allows some simple analytical manipulation (see Section 4.1). Under this assumption, we would have:

$$\Phi(x) = \frac{1}{\sqrt{2\pi} \sigma} e^{-\frac{(x-x_c)^2}{2\sigma^2}} \text{arcsec}^{-1} \quad (18)$$

where we adopt to measure x , x_c and σ in units of arcsec.

In this case, it is easy to show that the derivative of g_i in equation (12) can be written in a closed-form, as follows:

$$\frac{dg_i}{dx_c}(x_c) = \frac{1}{\sqrt{2\pi} \sigma} \left(e^{-\gamma(x_i^-)} - e^{-\gamma(x_i^+)} \right) \text{arcsec}^{-1} \quad (19)$$

where:

$$\gamma(x) = \frac{(x - x_c)^2}{2 \sigma^2} \quad (20)$$

with $x_i^- = x_i - \frac{\Delta x}{2}$ and $x_i^+ = x_i + \frac{\Delta x}{2}$.

Combining the results of equations (12), (18), (19) and (20) in (11) and converting to ADUs, we finally arrive at the following exact expression for the Cramér-Rao lower-bound in 1-D for a Gaussian PSF:

$$\sigma_{\text{CR}}^2 = 2\pi\sigma^2 \cdot \frac{B}{GF^2} \cdot \frac{1}{\sum_{i=1}^n \frac{\left(e^{-\gamma(x_i^-)} - e^{-\gamma(x_i^+)}\right)^2}{\left(1 + \frac{1}{\sqrt{2\pi}} \frac{F}{B} \int_{x_i - \frac{\Delta x}{2}}^{x_i + \frac{\Delta x}{2}} e^{-\gamma(x)} dx\right)}} \quad (21)$$

where we have assumed, for simplicity, that the background is uniform (and equal to B) under the PSF of the object. As noted by Winick (1986), this expression makes it explicit that the Cramér-Rao bound depends on F and B separately, and not just on the ratio F/B . If we adopt σ and Δx in unit of arcsec in the sky, then the square-root of equation (21) gives us the Cramér-Rao bound in units of arcsec directly.

In Figure 1 we show the results of evaluating equation (21) under the experimental setting proposed by Winick (1986), i.e., assuming a fixed set of F and B values (and therefore a constant ratio F/B), for different values of the detector pixel size Δx . In this figure we introduce the “Full-Width at Half-Maximum” ($FWHM$), usually termed as “image quality” at astronomical observing sites, which is related to the Gaussian σ through $FWHM = 2\sqrt{2\ln 2} \sigma$. Figure 1 is equivalent to Figure 1 in Winick (1986).

We note that, for a given continuous pixel x -coordinate on the array, the corresponding (integer) pixel ID, i , on the array, is given by:

$$i = INT(x + 0.5) \tag{22}$$

where the function INT represents the integer part of the argument. In this paper we adopt that pixel ID $i = 1$ has pixel coordinates $0.5 \leq x < 1.5$, pixel ID $i = 2$ has pixel coordinates $1.5 \leq x < 2.5$, and so on, following the convention of the IRAF package⁵. In this scheme, each pixel has width 1.0 in pixel x -coordinates, centered at $x = FLOAT(i)$, with upper/lower pixel boundaries given by $x_{\pm} = FLOAT(i) \pm 0.5$ (where the $FLOAT$ function converts an integer into a real number). The relationship between pixel x -coordinates and “physical” coordinates (projected onto the sky, as measured from the origin of the array), is given by $px = [(x - 0.5) \cdot \Delta x]$ arcsec.

3.3. The Cramér-Rao bound and dithering in undersampled images

An interesting feature is the effect on the predicted Cramér-Rao bound of pixel de-centering of the source. Figure 1 shows the effect of pixel de-centering for a $FWHM = 0.5$ arcsec, as a function of Δx . The fact that the Cramér-Rao bound *depends* on the location of the source itself was already pointed-out by Winick (1986), but this is evident from equations (10), (11) or (21), all of which explicitly depend on x_c . Of course, the effect is symmetrical with respect to the pixel center, so the impact of a de-centering of, e.g., +0.125 pix with respect to the pixel center is exactly the same as that of a de-centering of -0.125 pix, and (as long as the array properly samples the source), i.e. the effect is periodic (such that the Cramér-Rao bound is the same if the source is placed at

⁵IRAF is distributed by the National Optical Astronomy Observatories, which are operated by the Association of Universities for Research in Astronomy, Inc., under cooperative agreement with the National Science Foundation, see <http://iraf.noao.edu/>.

$x \pm FLOAT(n)$, where n is an arbitrary integer).

The important role of image de-centering in the case of undersampled images (such as those of *HST*, see below), has been demonstrated by Anderson & King (2000). They refer to the “pixel–phase error” as the systematic error in the derived center if a centering algorithm is used that does not properly account for the distribution of signal among pixels when the source is not centered in a pixel. On the other hand, the Cramér-Rao bound described here represents instead the precision, or random error, statistically attainable with an ideal, unbiased, centering algorithm.

The dotted line on Figure 1 is centered on a pixel, near the center of the array, the double-dotted-dashed line is for an offset of 0.125 pix, and the dot-dashed line is for a pixel de-centering of 0.25 pix. As it can be seen, the loss of astrometric accuracy as the pixel size increases, is less severe when the target is *not* at the center of a given pixel, but, rather, when it is offset from it. This is actually an intuitive result: For a given pixel size, when the source is not centered on a pixel, its flux is spread among more neighboring pixels, and therefore the source can be located more precisely. This result also implies that, for under-sampled systems, it is a good practice to “dither” the source a bit (even a fraction of a pixel) so that, in the end, the average Cramér-Rao bound is better than that if the source were located at the center of a pixel, a well known technique applied, e.g., to *HST* images (Anderson & King (2000), Fruchter & Hook (2002)). To quantify the effect of dithering, in Table 1 we show the Cramér-Rao bound for a source with a $FWHM = 0.5$ arcsec observed through detectors of pixel size $\Delta x = 0.5, 0.7$ and 0.9 arcsec, and when the source is centered and slightly de-centered by the amounts indicated in the table. As it can be seen from this table, for a pixel size that matches the $FWHM$, the change on the Cramér-Rao bound is small as a function of pixel offset. In the case of a 0.7 arcsec pixel size, a dither pattern including offsets of 0.125 and 0.25 pix, plus a central pointing, yields an average

Cramér-Rao bound of ~ 6.0 mas, which represents an almost 18% improvement over the (single) centered Cramér-Rao bound. For a 0.9 arcsec detector the effect is even more dramatic, yielding an almost 40% improvement.

Figure 1 also shows that, while the dithering technique offers a better asymptotic trend among all the values at large Δx (i.e., in the low-resolution regime), eventually, when Δx becomes too large, the astrometric accuracy deteriorates regardless of the relative position of the source with respect to the center of a pixel (even with dithering), as expected.

4. Astronomical application of the Cramér-Rao bound

We must note that F in equation (21) is the total source flux, which is independent of the pixel size on the detector, whereas B is, instead, the background level *in one pixel*. Therefore, as Δx becomes smaller and smaller, the *total* contribution from the background under the PSF of the source increases steadily (because B is fixed, and the number of pixels under the PSF increases), and the positional precision deteriorates (for a specific connection with the S/N ratio of the source, see equation (28) and the comments that follow that equation). On the other extreme, as Δx increases, we loose resolution and the positional precision also deteriorates. We get a “valley” which determines an optimum region Δx for a given set of F , B (and σ). While this setting is interesting in certain applications where the value of B is independent of the pixel size (e.g., military or day-time applications where the readout of the array is very fast, and the background is dominated by the electronics of the device, or when we are dominated by dark-current, see equation (23)), the situation in astronomical applications is quite different: In this case, the long readout times imply that, in most cases, the background is dominated by diffuse light coming from the sky, and not from the detector, and in this case the background in a given pixel *is not* independent of the pixel size, as assumed in the analysis by Winick (1986). The setting for evaluating

equation (21) must then be adapted to our case of interest, this is done in the next section.

As indicated in the previous paragraph, the correct expression for the (constant as a function of x , see equation (21)) background B contained in one pixel, is given in this case by:

$$B = f_s \Delta x + \frac{D + RON^2}{G} \text{ [ADU]} \quad (23)$$

where f_s is the sky background (in units of ADUs/arcsec), while D and RON are the dark-current and read-out noise of the detector (Howell 2013, pp. 222)⁶, per pixel, in units of e^- . In the paper by Winick (1986) it was assumed that $f_s \sim 0$ (true for very short exposure times), and we can see that, indeed, in this case, the background is independent of Δx . In what follow we will neglect the contribution from dark-current, which in current CCD detectors is negligible.

With this new prescription for B , and in order to evaluate the RHS of expression (21) for some astronomically interesting situations, it is also worth to develop some easily *measurable* form of “signal” and “noise” for our Gaussian source, as observed through our CCD detector. In this case one could define the signal S , as:

$$S = G \cdot F \cdot \int_{x_l}^{x_u} \Phi(x) dx \text{ [} e^- \text{]} \quad (24)$$

where x_l and x_u are suitably chosen (but arbitrary) apertures that include an appreciable fraction of the total flux of the star (we can not actually measure from $-\infty$ to $+\infty$ with a real detector, nor we want to do that since, in this formulation, the background

⁶See also, e.g., http://www.ucolick.org/~bolte/AY257/s_n.pdf, last accessed on December 2012.

will add-up to infinity over that aperture as well, see equations (26) and (27)). For the case of the Gaussian function adopted here, equation (18), it makes sense to perform an integration of the PSF that is symmetrical with respect to the center of the source, centered at x_c , in which case the signal can be written as:

$$S = G \cdot F \cdot P(u_+) [e^-] \quad (25)$$

where $P(u_+)$ is the probability integral⁷ evaluated at $u_+ = (x_u - x_c) / \sqrt{2} \sigma$, and where $x_u - x_c = x_c - x_l$.

The total noise, N , has contributions from the read-out-noise of the detector, the noise from the sky, and the noise from the source itself, all of which are assumed to follow Poisson statistics (in e^-), such that (see, e.g., Gilliland (1992)):

$$N = \sqrt{S + N_{\text{pix}} (G f_s \Delta x + RON^2)} [e^-] \quad (26)$$

where N_{pix} is the number of pixels under the same region in which the signal S was sampled, i.e., in the interval $[x_l, x_u]$, which is given by:

$$N_{\text{pix}} = \frac{x_u - x_l}{\Delta x} = \frac{2 \sqrt{2} \sigma u_+}{\Delta x} = \frac{u_+}{\sqrt{\ln 2}} \cdot \frac{FWHM}{\Delta x} \quad (27)$$

Combining equations (25), (26) and (27) we see that:

$$\frac{S}{N}(u_+) = \frac{P(u_+) \cdot F}{\sqrt{\frac{P(u_+) \cdot F}{G} + \frac{2 \sqrt{2} u_+ \cdot \sigma}{G \Delta x} (f_s \Delta x + \frac{RON^2}{G})}}$$

⁷The probability integral is defined as $P(u) = \frac{2}{\sqrt{\pi}} \int_0^u e^{-v^2} dv$

$$= \frac{P(u_+) \cdot F}{\sqrt{\frac{P(u_+) \cdot F}{G} + \frac{u_+}{\sqrt{\ln 2}} \frac{FWHM}{\Delta x} \left(f_s \Delta x + \frac{RON^2}{G}\right)}} \quad (28)$$

For example, for $P = 0.9$ (aperture containing 90% of the total flux), we have $u_+ \sim 1.164$ (the true “physical” aperture on the detector would be $\frac{1.164}{\sqrt{\ln 2}} \times FWHM \approx 1.40 \times FWHM$), whereas for $P = 0.99$ then $u_+ \sim 1.822$ (or $\frac{1.822}{\sqrt{\ln 2}} \times FWHM \approx 2.19 \times FWHM$). Because u_+ increases faster than $P(u_+)$ (which is bound to a maximum value of 1.0), we see that, for a given source, background, and detector, the S/N computed from equation (28) decreases as u_+ increases beyond the main core of the PSF. For example, for $\Delta x = 0.2$ arcsec, $G = 2 \text{ e}^-/\text{ADU}$, $RON = 5 \text{ e}^-$, $f_s = 2000 \text{ ADU/arcsec}$, $F = 5000 \text{ ADU}$, and $FWHM = 1.0$ arcsec, then for $P = 0.9$, $S/N \sim 74$, whereas for $P = 0.999$ (for which $u_+ \sim 2.33$), $S/N \sim 68$. As was explained before, we note that equation (21) does not depend directly on the S/N .

Equation (28) is interesting since it explicitly shows that, as Δx becomes smaller and smaller, the RON term starts to dominate over the sky background in its contribution to the total noise, the impact of which, on the Cramér-Rao bound, has already been mentioned in Subsection 3.2. However, when Δx increases, the sky background becomes the dominant source of background noise, and the total noise becomes *independent* of the array pixel size. Also, this equation clearly shows the classical result that, as an image becomes more spread (larger $FWHM$, or worse image quality) the S/N deteriorates, for a fixed total flux F , because of the larger contribution from the sky and the (larger number of) pixels underneath the aperture: As we shall see, the $FWHM$ has a very relevant impact on the Cramér-Rao bound (see, e.g., equation (45)).

Figure 2 shows the result of evaluating equation (21) under the assumption of a background given by equation (23) for a set of representative values. An interesting point here is that, at very small values of Δx we still see the “upturn” in the Cramér-Rao

lower bound seen in Figure 1, but it has a much smaller effect. Of course, the reason for this upturn is the prevalence of the *RON* over the sky background indicated in the previous paragraph, when Δx becomes extremely small. As we shall see (equation (45)), the Cramér-Rao bound goes as Δx^{-1} for small S/N and small pixels, a feature clearly seen in Figure 2. Otherwise we see a broad region that exhibits a rather smooth and steady decrease in positional precision when Δx becomes larger and larger, and a rather steep increase when Δx increases beyond the *FWHM*. The overall effects of pixel de-centering are qualitatively similar to those already presented in Figure 1, and are thus not repeated in this figure. For very large S/N , equation (45) predicts that the Cramér-Rao bound becomes rather insensitive to Δx , which also coincides with the behavior in Figure 2.

An interesting prediction of equation (21) is that high-resolution imaging in low-background, even for under-sampled images (e.g., HST), is better than imaging with larger aperture ground-based telescopes, not under-sampled, due to the worse *FWHM* and higher-background of the latter, a well-known fact by people doing astrometry with HST (provided, of course, that systematic effects are well understood, e.g., a particularly challenging situation with HST data is the account of time-dependent charge-transfer efficiency corrections, for details see, e.g., Bristow et al. (2005), especially their Figure 4, or Bristow et al. (2006), especially their Figure 10). For example, for the same detector parameters as those adopted in Figure 2, and $F = 10\,000$ (which for a Gaussian PSF leads to maximum flux in the central pixel of $\sim 1\,700$ ADU (see Section 4.1 and equation (44)), $f_s = 3\,000$ ADU/pix, and $FWHM = 0.45$ arcsec, the Cramér-Rao bound is ~ 1.7 mas (with $\Delta x = 0.08$ arcsec). These (source & image) values are similar to those of the QSOs used in the astrometric study by Méndez et al. (2010) (see their Table 1) and Méndez et al. (2011), which demonstrated a single-measurement astrometric precision of 1.5 mas (see Section 3.2 in Méndez et al. (2010)) with the NTT (3.5m aperture) telescope and SUSI2 imager. On the other hand, for HST with $f_s = 30$ ADU/pix and $FWHM = 0.15$ arcsec, then the

Cramér-Rao bound is ~ 0.2 mas (in this case $\Delta x = 0.1$ arcsec), whereas Piatek et al. (2002) reported a single-measurement precision of 0.25 mas (in our calculation of the Cramér-Rao bound for HST we have approximately taken into account the aperture difference between the NTT and HST, and the different exposure times for the same QSOs adopted in these two studies, from Table 1 in Piatek et al. (2002)).

4.1. The Cramér-Rao bound in the small pixel (high resolution) approximation

Under certain circumstances, the summation in the denominator of the RHS of equation (10) can be approximated into an integral, which allows us to explore the behavior of the Cramér-Rao bound in a more explicit manner. Indeed, we see from equations (12) and (18) that the application of the mean-value theorem when $\Delta x/\sigma \ll 1$ implies that $\tilde{F}_i \equiv \tilde{F} \cdot g_i(x_c) \approx \tilde{F} \cdot \Phi(x_i) \cdot \Delta x$. In this case, for a Gaussian PSF, it is easy to show that:

$$\frac{d\tilde{F}_i}{dx_c}(x_c) \equiv \tilde{F} \frac{dg_i}{dx_c}(x_c) = \frac{(x_i - x_c)}{\sigma^2} \cdot \tilde{F}_i \quad (29)$$

Replacing the RHS of equation (29) into the RHS of equation (10) we have:

$$\sigma_{\text{CR}}^2 = \sigma^4 \cdot \frac{1}{\sum_{i=1}^n (x_i - x_c)^2 \cdot \frac{\tilde{F}_i^2}{(\tilde{F}_i + \tilde{B}_i)}} \quad (30)$$

Let us have a closer look at the (dimensionless) \tilde{F}_i and \tilde{F}_i^2 terms in the RHS of equation (30). For our Gaussian function we will have:

$$\tilde{F}_i \equiv \tilde{F} \int_{x_i - \frac{\Delta x}{2}}^{x_i + \frac{\Delta x}{2}} \Phi(x) dx = \frac{\tilde{F}}{\sqrt{2\pi}\sigma} \int_{x_i - \frac{\Delta x}{2}}^{x_i + \frac{\Delta x}{2}} e^{-\frac{(x-x_c)^2}{2\sigma^2}} dx \quad (31)$$

which, in the small pixel size approximation becomes:

$$\tilde{F}_i \approx \frac{\tilde{F}}{\sqrt{2\pi}\sigma} \cdot e^{-\frac{(x_i-x_c)^2}{2\sigma^2}} \cdot \Delta x \quad (32)$$

$$= \tilde{F}_{\max} \cdot e^{-\frac{(x_i-x_c)^2}{2\sigma^2}} \quad (33)$$

where \tilde{F}_{\max} is the (dimensionless) maximum flux, which will occur at a certain pixel j that satisfies the condition $x_j - \Delta x/2 \leq x_c < x_j + \Delta x/2$.

Equation (32) prompts us to define a *new function*, which describes the distribution across pixels, in the small-pixel approximation, of the *square of the flux* that appears in equation (30), as:

$$\tilde{F}_i^2 = \hat{F}^2 \cdot e^{-\frac{(x_i-x_c)^2}{\sigma^2}} \cdot \Delta x \quad (34)$$

where \hat{F}^2 is a proper normalization factor (in units of arcsec^{-1} , see below).

Combining equations (33) and (34) in equation (30), and considering that Δx is very small, we have:

$$\sigma_{\text{CR}}^2 = \frac{\sigma^4}{\hat{F}^2} \cdot \lim_{\Delta x \rightarrow 0} \frac{1}{\sum_{i=1}^n \frac{(x_i - x_c)^2 \cdot e^{-\frac{(x_i-x_c)^2}{\sigma^2}}}{(\tilde{F}_i + \tilde{B}_i)} \cdot \Delta x} = \frac{\sigma^4}{\hat{F}^2} \cdot \frac{1}{\int_{-\infty}^{+\infty} \frac{(x - x_c)^2 \cdot e^{-\frac{(x-x_c)^2}{\sigma^2}}}{(\tilde{F}(x) + \tilde{B}(x))} dx} \quad (35)$$

Taking into account the definition of \tilde{F}_{\max} on equation (33), from equation (34) we will have that $\tilde{F}_{\max}^2 \equiv \tilde{F}_j^2 \approx \hat{F}^2 \cdot \Delta x$, where we have used the fact that, since Δx is very small, then $x_j \approx x_c$. Replacing this approximation and equation (33) into equation (35) we get for the Cramér-Rao bound in the small-pixel approximation:

$$\sigma_{\text{CR}}^2 = \frac{\sigma^4}{\tilde{F}_{\text{max}}^2} \cdot \frac{\Delta x}{\int_{-\infty}^{+\infty} \frac{(x - x_c)^2 e^{-\frac{(x-x_c)^2}{\sigma^2}}}{\left(\tilde{F}_{\text{max}} \cdot e^{-\frac{(x-x_c)^2}{2\sigma^2}} + \tilde{B}(x)\right)} dx} \equiv \frac{\sigma^4}{\tilde{F}_{\text{max}}^2} \cdot \frac{\Delta x}{I} \quad (36)$$

where we note that (the trivial definition of) integral I has units of arcsec³.

This formula is only valid under the assumption of small pixels, so, in a general application, equation (10) should be used instead, or equation (21) for a Gaussian PSF. However, the truly interesting aspect of this equation is that it can be explicitly evaluated in two extreme cases: When the detection is dominated by the source, and when it is dominated by the background. This is done in the next subsections.

4.1.1. Weak source

When the background dominates, then $\tilde{F}_{\text{max}} \ll \tilde{B}(x)$. In this case we would have:

$$I = \int_{-\infty}^{+\infty} \frac{(x - x_c)^2 e^{-\frac{(x-x_c)^2}{\sigma^2}}}{\left(\tilde{F}_{\text{max}} \cdot e^{-\frac{(x-x_c)^2}{2\sigma^2}} + \tilde{B}(x)\right)} dx \approx \int_{-\infty}^{+\infty} \frac{(x - x_c)^2 e^{-\frac{(x-x_c)^2}{\sigma^2}}}{\tilde{B}(x)} dx \quad (37)$$

If we assume an approximately constant background under the PSF of the target then:

$$I = \frac{1}{\tilde{B}} \int_{-\infty}^{+\infty} (x - x_c)^2 e^{-\frac{(x-x_c)^2}{\sigma^2}} dx = \frac{\sqrt{\pi}}{2} \cdot \frac{\sigma^3}{\tilde{B}} \quad (38)$$

Therefore, in this case, replacing I into equation (36) and re-arranging terms, the Cramér-Rao bound becomes:

$$\sigma_{\text{CR}}^2 = \frac{2}{\sqrt{\pi}} \cdot \frac{\tilde{B}}{\tilde{F}_{\text{max}}^2} \cdot \Delta x \cdot \sigma$$

$$= \frac{1}{\sqrt{2\pi \ln 2}} \cdot \frac{B}{G F_{\max}^2} \cdot \Delta x \cdot FWHM \quad (39)$$

The (pedagogical) use of this equation is that it allows us to draw some basic conclusions regarding the expected positional accuracy in this regime. First, because $\tilde{F}_{\max} \ll \tilde{B}(x)$ we predict, in general, a rather large positional uncertainty, as expected, due to the low S/N of the source. Furthermore, the accuracy will improve proportionally to F_{\max}^{-1} , in agreement with equation (10) of Lee and van Altena (1983) (compare also the first line of equation (39) with equation (7) in Auer and van Altena (1978)). Furthermore, as intuitively expected, the accuracy deteriorates for a larger background, coarser pixel size, or for lower-quality images (or sites), but relatively slowly: Only as the square root of these parameters.

4.1.2. Strong source

In this case, the signal from the source dominates over the background, i.e., $\tilde{F}_{\max} \gg \tilde{B}(x)$, and the approximation for I becomes:

$$I = \int_{-\infty}^{+\infty} \frac{(x - x_c)^2 e^{-\frac{(x-x_c)^2}{\sigma^2}}}{\left(\tilde{F}_{\max} \cdot e^{-\frac{(x-x_c)^2}{2\sigma^2}} + \tilde{B}(x) \right)} dx \approx \frac{1}{\tilde{F}_{\max}} \int_{-\infty}^{+\infty} (x - x_c)^2 e^{-\frac{(x-x_c)^2}{2\sigma^2}} dx \quad (40)$$

Evaluating the definite integral we have:

$$I = \sqrt{2\pi} \cdot \frac{\sigma^3}{\tilde{F}_{\max}} \quad (41)$$

Replacing this value for I into equation (36) we end up with:

$$\begin{aligned}
 \sigma_{\text{CR}}^2 &= \frac{1}{\sqrt{2\pi}} \cdot \frac{1}{F_{\text{max}}} \cdot \Delta x \cdot \sigma \\
 &= \frac{1}{4\sqrt{\pi \ln 2}} \cdot \frac{1}{G F_{\text{max}}} \cdot \Delta x \cdot FWHM
 \end{aligned} \tag{42}$$

We see that, in this regime, the ultimate positional accuracy is proportional to $F_{\text{max}}^{-1/2}$, similarly to what was found by Lee and van Altena (1983) (see their equation (13)). Again, the accuracy deteriorates slowly for coarser pixel size and for lesser-quality images, but in this case the background level, formally, plays no role in the expected accuracy.

4.1.3. Limiting cases as a function of total flux

Equations (39) and (42) are a bit misleading because, by definition, F_{max} depends itself on the adopted value for Δx and, therefore, needs to be evaluated in each particular case. However, in the small pixel approximation, one can find an approximate relationship between the total flux F (which is independent of Δx) and F_{max} . Indeed, assuming, as done before, that, $x_j \approx x_c$, then:

$$F_{\text{max}} \equiv F_j = \frac{F}{\sqrt{2\pi}\sigma} \int_{x_j - \frac{\Delta x}{2}}^{x_j + \frac{\Delta x}{2}} e^{-\frac{(x-x_c)^2}{2\sigma^2}} dx \tag{43}$$

$$\approx \frac{F}{\sqrt{2\pi}} \cdot \frac{\Delta x}{\sigma} \tag{44}$$

Replacing equation (44) into equations (39) and (42) we have:

$$\sigma_{\text{CR}}^2 \approx \begin{cases} \frac{\sqrt{\pi}}{2(2 \ln 2)^{3/2}} \cdot \frac{B}{G F^2} \cdot \frac{FWHM^3}{\Delta x} & \text{if } F \ll B \\ \frac{1}{8 \ln 2} \cdot \frac{1}{G F} \cdot FWHM^2 & \text{if } F \gg B \end{cases} \tag{45}$$

Interestingly, we now see that the positional accuracy should deteriorate linearly with the $FWHM$ of the image for strong sources, but it will not otherwise depend on the array pixel size. However, for weak sources, the dependence on the $FWHM$ is not only steeper but, also, the finer the pixel size, the larger the expected positional uncertainty. This latter result should also be intuitive since, when we are dominated by the background, the more pixels we have under the PSF, the larger the contribution of the background will be, to the point of significantly perturbing the final positional accuracy. Equivalently, note that the term $B/\Delta x$ is the background per unit area (see equation (23)): The larger this value becomes, we indeed expect a larger positional uncertainty, as shown by the first line on equation (45). The behavior depicted by equation (45) is similar to that found by King (1983): For sources where the background dominates, his equation (23) predicts that the positional uncertainty goes as \sqrt{B}/F , whereas when the background is negligible, his equation (24) shows that the positional uncertainty increases as $1/\sqrt{F}$. Similarly, Lindegren (1978) (see also van Altena and Fomalont (2013, pp. 127)) finds that for a seeing-limited image with no background, the limiting astrometric precision goes as $FWHM/(S/N)$, which is equivalent to equation (45) for the case $F \gg B$, when $S/N \sim \sqrt{F}$, see equation (28)). All these predictions coincide with those from our equation (45). Finally, and as already noted in Section 4, the general trends seen in Figure 2 are well explained by equation (45).

4.1.4. Range of use of the high resolution Cramér-Rao bound

Besides their qualitative usefulness, what is the range of applicability of equations (39) and (42), or (45)? For illustration purposes, in Table 2 we compare the values predicted by these equations, with the “exact” prediction from equation (21), for some representative values of the parameters. From this Table we can see that, even for relatively large pixels, in comparison with the $FWHM$, these equations predict very reasonable values in

comparison with the “exact” value, as long as we respect the conditions for F/B under which equations (39) and (42) were derived. The second and third lines show that, indeed, as predicted by equation (45), the Cramér-Rao bound does not depend on B . The third and fourth lines show that in the high- S/N regime the Cramér-Rao bound goes linearly with the $FWHM$, while a comparison of the first and fifth line demonstrate that in the low- S/N case the Cramér-Rao bound varies as the ratio $FWHM^2/\Delta x$, as shown by equation (45). Finally, in the last two lines of the table, we show a case when equation (45) fails miserably, i.e., for an intermediate S/N value.

4.1.5. *A simplified extension to the 2-D Case*

It can be intuitively argued from either equations (39) and (42), or equation (45), that in the 2-D case the numerical factors in front of these equations will be somewhat altered, but their basic dependence on F and B should be basically maintained, as already indicated by a comparison of our results to the 2-D results by Auer and van Altena (1978), Lee and van Altena (1983) and King (1983) noted in Sections 4.1.1, 4.1.2 and 4.1.3. For example, if the source is relatively symmetrical, such that we can replace an x-y integration (similar to that of equation (36) but in the two array dimensions x, y) by a polar-radial integration, we will end up with a Δr instead of a Δx , or even something like $\sqrt{\Delta x \cdot \Delta y}$ for a non-square pixel array. Therefore, even though our present results are based purely on a 1-D array, they have a very interesting predictive power, a point to which we will return in Section 5.3 (see also Table 4).

5. Comparing the Cramér-Rao bound with the performance of practical estimators

Let us remember that the necessary and sufficient condition for the existence of an estimator that achieves the Cramér-Rao bound is that the likelihood function can be decomposed as in equation (5). Unfortunately, equation (8) does not offer, in general, the normal form of equation (5), and consequently no estimator achieves the Cramér-Rao lower bound.

To further explore this, it is illustrative to consider the high-resolution regime of Section 4.1, in which case equation (29) holds. Replacing this into equation (8), and re-arranging some terms, we have:

$$\frac{d \ln L(I_1, \dots, I_n; x_c)}{dx_c} = \sum_{i=1}^n \frac{\tilde{F}_i}{\sigma^2} \cdot \left(\frac{I_i}{\tilde{F}_i + \tilde{B}_i} - 1 \right) \cdot (x_i - x_c) \quad (46)$$

Note that although the expression in equation (46) is reminiscent of equation (5), the factor attributed to $A(\theta)$ in equation (46), is a function of the data (I_i, x_i) , and therefore does not fulfill the decomposition in equation (5). Consequently, even under the high resolution approximation, there is no estimator that achieves the Cramér-Rao bound. This situation supports and justifies the adoption of *alternative criteria* for position estimation, maximum likelihood and the classical least squares being two of the more commonly used approaches adopted. These are reviewed in the following subsections.

5.1. Maximum Likelihood

Given the flux values I_1, \dots, I_n , the maximum-likelihood (ML) estimate of the position x_c is obtained through the following rule:

$$\hat{x}_{cML}(I_1, \dots, I_n) = \arg \max_{x_c} \ln L(I_1, \dots, I_n; x_c) \quad (47)$$

where “arg max” represents the argument that maximizes the expression. Imposing the first order condition on this optimization problem, it reduces to satisfying the condition $\frac{d \ln L(I_1, \dots, I_n; x_c)}{dx_c} = 0$, and, consequently, we can work with the general expression in equation (7). We note, from that equation, that the term in the brackets given by $\sum_{i=1}^n \lambda_i(x_c) \equiv \tilde{F} + \tilde{B}$ is independent of x_c , and consequently its derivative is zero. Therefore the ML condition becomes:

$$\frac{d \ln L(I_1, \dots, I_n; x_c)}{dx_c} \equiv \sum_{i=1}^n I_i \cdot \frac{1}{\lambda_i(x_c)} \cdot \frac{d\lambda_i(x_c)}{dx_c} = \frac{1}{\sigma^2} \sum_{i=1}^n I_i \cdot \frac{\tilde{F}_i(x_c)}{\tilde{F}_i(x_c) + \tilde{B}_i(x_c)} \cdot (x_i - x_c) = 0 \quad (48)$$

where we have used the high-resolution approximation, equation (29). In general, this condition does not offer a closed-form solution (note that the dependency of \tilde{F}_i on x_c could be quite complex), consequently numerical gradient-descent methods need to be implemented. Nevertheless, in the signal-dominated regime, when $\tilde{F}_i \gg \tilde{B}_i$, it is straightforward to show that equation (48) reduces to the classical moment solution, i.e.:

$$\hat{x}_{cML} = \frac{\sum_{i=1}^n I_i \cdot x_i}{\sum_{i=1}^n I_i} \quad (49)$$

In general, the formal solution to equation (48) in the high-resolution regime offers a simple relationship to implement a recursive algorithm that satisfies the ML estimate, given by:

$$\hat{x}_{cML} = \frac{\sum_{i=1}^n w_i(x_c) \cdot I_i \cdot x_i}{\sum_{i=1}^n w_i(x_c) \cdot I_i} \quad (50)$$

where the weights $w_i(x_c) \equiv \frac{\tilde{F}_i(x_c)}{\tilde{F}_i(x_c) + \tilde{B}_i}$.

To conclude this subsection, we must mention that it is well-known that in the setting of independent and identically distributed measurements, the ML estimate is asymptotically unbiased and efficient (Stuart, et al. 2004, Chap. 18). In other words, as the number of samples increases, the variance tends to the Cramér-Rao bound and consequently the ML is asymptotically optimal (in the sense of achieving the minimum variance bound). However, the astrometry setting is different as the measurements (fluxes) follow a Poisson distribution with parameters that are position dependent (see Section 2.2), and consequently the ML is not necessarily efficient in this statistical sense.

5.2. Least Squares

Given the flux values I_1, \dots, I_n , the (weighted) least square (LS) estimate of the position x_c is given by the following decision-rule:

$$\hat{x}_{cLS}(I_1, \dots, I_n) = \arg \min_{x_c} \sum_{i=1}^n \frac{(I_i - a_i(x_c))^2}{b_i(x_c)} \quad (51)$$

being $a_i(x_c) \equiv \mathbb{E}(I_i) = \lambda_i(x_c)$ and $b_i(x_c) \equiv Var(I_i) = \lambda_i(x_c)$ for all i .⁸ The unweighted LS estimate assumes instead that $b_i = 1$, where no variance normalization is considered at

⁸Note that the ML reduces to the LS estimate when the data follows a Gaussian distribution.

all.

If we define $E_{LS}(I_1, \dots, I_n; x_c) \equiv \sum_{i=1}^n (I_i - \lambda_i(x_c))^2$, then the first-order condition over the unweighted LS estimate implies that:

$$\frac{dE_{LS}(I_1, \dots, I_n; x_c)}{dx_c} = \sum_{i=1}^n (I_i - \lambda_i(x_c)) \cdot \frac{d\lambda_i(x_c)}{dx_c} = 0 \quad (52)$$

Hence, using again the high-resolution regime (equation (29)), this condition implies that:

$$\frac{dE_{LS}(I_1, \dots, I_n; x_c)}{dx_c} = \sum_{i=1}^n \frac{\tilde{F}_i}{\sigma^2} \cdot (I_i - \lambda_i) \cdot (x_i - x_c) = 0 \quad (53)$$

and, consequently, the problem reduces to solve the equation:

$$\hat{x}_{cLS} = \frac{\sum_{i=1}^n \tilde{F}_i \cdot (I_i - \lambda_i(x_c)) \cdot x_i}{\sum_{i=1}^n \tilde{F}_i \cdot (I_i - \lambda_i(x_c))} \quad (54)$$

Note that this expression is the counterpart of equation (50) for the ML estimate, emphasizing that these two techniques offer *different* estimates of the position in the parametric setting of astrometry. Again the solution of (54) involves the use of numerical methods, as, in general, no closed-form solution can be derived from it.

5.3. Numerical results

In this section we present some results from numerical experiments for the standard deviation of the astrometric position of a 1-D Gaussian source sampled by a linear detector.

The goal of these experiments is to compare the performance of the ML and LS solutions described in the previous subsections, to the theoretical Cramér-Rao bound, under different assumptions regarding the detector and the source.

Basically, we start by adopting a set of values for the gain and read-out noise of the detector, as well as its pixel size and number of pixels. For a source with a Gaussian PSF, we specify its width, the maximum flux at the central pixel and its center location (x_c). For the background, we adopt a certain (fixed) value per pixel. The total flux of the source (in ADUs) is obtained through equation (43) by direct integration of the Gaussian PSF given the adopted values for Δx , x_c and σ . We generate many possible “observations” for the same combination of parameters, using a random-number generator driven by a Poisson distribution using the *poidev*, *gammaln*, and *ran1* routines explained in Press et al. (1992). We note that we transform all the ADUs (source and background) to units of e^- using the adopted gain, before randomizing the data. When generating the data, we also consider the read-out noise and the “digitization noise” (see, e.g, Gilliland (1992)). On output we have an array of pixel positions (1 to n) and their corresponding fluxes.

After generating a (large) number of simulations for a given set of parameters, we compute the value of x_c using a ML and a LS (weighted and unweighted) procedure. Because we are operating in the 1-D case, where we are estimating the object’s position exclusively, all the other parameters were assumed to be known, and fed to the routine that searched for the value of x_c , using either equation (47) in the case of ML or equation (51) in the case of LS. To estimate the optimum number of simulations required to obtain a stable solution, we computed a very large number of simulations for our first set, and then calculated the mean of the recovered x_c and its standard deviation, σ_{x_c} , as a function of the number of simulations. The optimum value for the number of simulations should render a set of values (x_c , σ_{x_c}) that do not depend appreciably (within their statistical uncertainty)

on adding more simulations. For our simulations, this number turned out to be ~ 250 simulations per set.

In Table 3 we present the standard deviation from the simulations, σ_{x_c} , for a number of representative cases, as well as the calculated Cramér-Rao minimum variance bound based on equation (21), denoted by σ_{CR} . In all cases we adopted an array size of 100 pixels that properly covers the PSF, a pixel size of 0.2 arcsec, a detector $RON = 5 e^-$, a (fixed) sky background of 300 ADU per pixel, and a Gaussian source with a $FWHM = 1$ arcsec.

To our surprise, the results on Table 3 indicate that the performance of the ML and LS estimators are almost equal to the Cramér-Rao lower bound. This is a remarkable result, and it validates the predictive power of the Cramér-Rao bound and its use as a benchmark indicator in astrometry. From the theoretical side, we formally showed (Section 5, equation (46)) that the Cramér-Rao bound for astrometry can not be achieved. Our numerical results suggest then that, both, the ML and the LS methods (which are widely used in astrometry), are very efficient in the sense of asymptotically (with the number of measurements) approaching the Cramér-Rao bound. Proving this conjecture is an interesting topic of further work which will help us to explain the results obtained, and further consolidate the use the Cramér-Rao bound for performance analysis. A possible explanation, valid in the 1-D case, has been proposed in Section 3.1: This explanation however is not valid in a general situation, where one needs to simultaneously estimate astrometric and photometric parameters, the subject of which will be further explored in a forthcoming paper. We also note from Table 3 that the ML is as good as, or even better in some cases, than the LS and WLS estimators.

We finally compare the predictions of the Cramér-Rao lower bound to the performance of some 2-D digital centering algorithms applied to simulated stellar images, reported by Stone (1989). As argued in Section 4.1.5 we should expect that our results from the 1-D

case should not significantly differ from those of a 2-D case when the source is symmetrical. Indeed, Stone (1989) adopted for his simulations symmetrical Gaussian sources (his equation (1)) on a flat background. We have read approximately from his Figures 2 to 5 the results for the *minimum* rms (over different profile fitting methods) of the positional uncertainty from his 2-D numerical simulations for some representative values of the total flux F , this are tabulated in our Table 4 under the label σ_{st} , in units or arcsec. For each of these values we have computed the predicted Cramér-Rao bound using our equation (21), and adopting the same values for F , B , $FWHM$, and Δx used by Stone (1989) for each of his simulations. These values are denoted by σ_{CR} in Table 4, also in units or arcsec. As can be seen from this Table, our predictions are extremely encouraging: In all cases our computed Cramér-Rao bound is smaller than (although typically close to) the results from the “measured” standard deviation of the position (derived from the 2-D simulations). Furthermore, as indicated in Section 5.1 (specially equation (50)), when $F \gg B$ we would expect that the ML estimate approaches the moment solution, which is indeed the case as seen from Table 4 (see also Figures 2 and 3 for large “counts in image” in Stone (1989)).

6. Conclusions

Our results indicate that we have found in the Cramér-Rao lower variance bound a very powerful astrometric “benchmark” estimator concerning the maximum expected positional precision for a point source, given a prescription for the source, the background, the detector characteristics, and the detection process.

We regard as particularly interesting, pedagogical, and as a “back of an envelope” estimation tool, the set of equations (45) which, albeit derived in the high-resolution regime, are actually quite resilient to this condition, and thus provide reasonable expectations for the astrometric precision.

In a forthcoming paper we will formally extend our analysis to the 2-D case for the estimation of (x, y) coordinates in a more realistic pixel array. It has been argued however (see Sections 4.1.5 and 5.3) that, as long as the PSF is reasonably symmetric, the results on equation (45) are not likely to change much in this case. In particular, the result that for background-dominated sources the Cramér-Rao lower bound goes as B/F^2 , while when the background is negligible, this maximum achievable precision goes as F^{-1} should still hold in the 2-D case.

Also, it would be interesting to study the sensitivity of the Cramér-Rao bound to other PSF shapes. We note however that the results by King (1983), which coincide with our own results (see Section 4.1.3), have been derived from a different PSF (his equation (10)). King (1983) argues that, by using a Gaussian instead, only minor differences in the numerical coefficients in his equations (23) and (24) appear.

Other factors to consider in a more realistic application include the existence of a strong gradient in the background under the object's PSF, which will tend to bias the derived astrometry, and possibly also affect the Cramér-Rao estimate (throughout this paper we have assumed that the background is uniform, but an extension to a highly variable background is straightforward to implement, starting from equation (11)). Also, in the case of severely under-sampled images, the issue of intra-pixel response function has been demonstrated to be significant (see, e.g., Figure 1 in Adorf (1996)), and should be included in the analysis.

Eventually, one would like to be able to compute the Cramér-Rao bound in cases where there is a simultaneous joint estimation of the photometric (source and background), and astrometric (position, width of the PSF) parameters, which would for sure require non-linear, possibly iterative, numerical methods, in which careful attention should be given to numerical stability issues, and proper handling of observational errors - this constitutes

the long-term goal of our research.

RAM acknowledges partial support from the “Center of Excellence in Astrophysics and Associated Technologies” (PFB 06) - CONICYT. JFS acknowledges support from FONDECYT - CONICYT grant #1110145. The authors would also like to acknowledge Prof. William F. van Altena for many useful comments on an earlier version of this paper, and an anonymous referee for his/her many corrections and suggestions of style, and for highlighting some aspects of our work that led to Section 3.3.

A. Derivation of the Fisher information about x_c

We start from the expression in equation (7):

$$\frac{d \ln L(I_1, \dots, I_n; x_c)}{dx_c} = \sum_{i=1}^n I_i \cdot \frac{1}{\lambda_i(x_c)} \cdot \frac{d\lambda_i(x_c)}{dx_c} \quad (\text{A1})$$

where, without any loss of generality, we have assumed that $\sum_{i=1}^n \lambda_i(x_c)$ is constant, independent of the parameter x_c (see details on Section 5.1). Then, the Fisher information about x_c can be obtained as follows (see equation (4)):

$$\begin{aligned} \mathcal{I}_{x_c}(n) &\equiv \mathbb{E}_{I_1, \dots, I_n} \left(\left(\frac{d}{dx_c} \ln L(I_1, \dots, I_n; x_c) \right)^2 \right) \\ &= \mathbb{E}_{I_1, \dots, I_n} \left(\sum_{i=1}^n \sum_{j=1}^n \frac{I_i \cdot I_j}{\lambda_i(x_c) \cdot \lambda_j(x_c)} \cdot \frac{d\lambda_i(x_c)}{dx_c} \cdot \frac{d\lambda_j(x_c)}{dx_c} \right) \\ &= \mathbb{E}_{I_1, \dots, I_n} \left(\sum_i \left(\frac{I_i}{\lambda_i(x_c)} \cdot \frac{d\lambda_i(x_c)}{dx_c} \right)^2 \right) + \mathbb{E}_{I_1, \dots, I_n} \left(\sum_i \sum_{j \neq i} \frac{I_i \cdot I_j}{\lambda_i(x_c) \cdot \lambda_j(x_c)} \cdot \frac{d\lambda_i(x_c)}{dx_c} \cdot \frac{d\lambda_j(x_c)}{dx_c} \right) \\ &= \sum_i \frac{(\lambda_i(x_c) + \lambda_i(x_c)^2)}{\lambda_i(x_c)^2} \cdot \left(\frac{d\lambda_i(x_c)}{dx_c} \right)^2 + \sum_i \sum_{j \neq i} \frac{d\lambda_i(x_c)}{dx_c} \cdot \frac{d\lambda_j(x_c)}{dx_c} \\ &= \sum_i \frac{1}{\lambda_i(x_c)} \cdot \left(\frac{d\lambda_i(x_c)}{dx_c} \right)^2 + \sum_i \left(\frac{d\lambda_i(x_c)}{dx_c} \right)^2 + \sum_i \sum_{j \neq i} \frac{d\lambda_i(x_c)}{dx_c} \cdot \frac{d\lambda_j(x_c)}{dx_c} \\ &= \sum_i \frac{1}{\lambda_i(x_c)} \cdot \left(\frac{d\lambda_i(x_c)}{dx_c} \right)^2 + \left(\sum_i \frac{d\lambda_i(x_c)}{dx_c} \right)^2 \\ &= \sum_i \frac{1}{\lambda_i(x_c)} \cdot \left(\frac{d\lambda_i(x_c)}{dx_c} \right)^2 + \left(\frac{d}{dx_c} \sum_{i=1}^n \lambda_i(x_c) \right)^2 = \sum_{i=1}^n \frac{1}{\lambda_i(x_c)} \cdot \left(\frac{d\lambda_i(x_c)}{dx_c} \right)^2 \quad (\text{A2}) \end{aligned}$$

where we have used the fact that, for a Poisson distribution, $\lambda_i = \mathbb{E}(\text{Var}(I_i)) \equiv \mathbb{E}(I_i - \lambda_i)^2 = \mathbb{E}(I_i^2) - \lambda_i^2$.

REFERENCES

- Adorf, H.-M. 1996, *Astronomical Data Analysis Software and Systems V*, 101, 13
- Anderson, J., & King, I. R. 2000, *PASP*, 112, 1360
- Auer, L. H., van Altena, W. 1978, *AJ*, 83, 531
- Bastian, U. 2004. GAIA technical note, 2004BASNOCODE. Available at http://www.rssd.esa.int/doc_fetch.php?id=2939027 (last accessed on November 2012)
- Bendinelli, O., Zavatti, F., & Parmeggiani, G. 1988, *Journal of Astrophysics and Astronomy*, 9, 17
- Bristow, P., Piatek, S., & Pryor, C. 2005, *Space Telescope European Coordinating Facility Newsletter*, 38, 12
- Bristow, P., Kerber, F., & Rosa, M. R. 2006, *The 2005 HST Calibration Workshop: Hubble After the Transition to Two-Gyro Mode*, 299
- Cramér, H. 1946, *Mathematical Methods of Statistics*. Princeton University Press, New Jersey
- Fruchter, A. S., & Hook, R. N. 2002, *PASP*, 114, 144
- Gilliland, R. L. 1992, *Astronomical CCD Observing and Reduction Techniques*, 23, 68
- Howell, S.B. 2006, *Handbook of CCD Astronomy*, 2nd Edition, Cambridge Observing Handbooks for Research Astronomers. Cambridge University Press
- Howell, S.B. 2013. In *Astrometry for Astrophysics*, William F. van Altena (ed.). Cambridge University Press, Chapter 14

- Jakobsen, P., Greenfield, P., & Jedrzejewski, R. 1992, *A&A*, 253, 329
- King, I. R. 1971, *PASP*, 83, 199
- King, I. R. 1983, *PASP*, 95, 163
- Lee, J.-F., van Altena, W. 1983, *AJ*, 88, 1683
- Lindgren, L. 1978, *IAU Colloq. 48: Modern Astrometry*, 197
- Lindgren, L. 1997, *GAIA Technical Note “Astrometric precision for direct fringe detection”*
- Lindgren, L. 2005, *The Three-Dimensional Universe with Gaia*, 576, 29
- Lindgren, L. 2010, *ISSI Scientific Reports Series*, 9, 279
- Mackay, C. D. 1986, *ARA&A*, 24, 255
- Méndez, R. A., Costa, E., Pedreros, M. H., et al. 2010, *PASP*, 122, 853
- Méndez, R. A., Costa, E., Gallart, C., et al. 2011, *AJ*, 142, 93
- Meyer, S.L. 1992. *Data Analysis for Scientists and Engineers*, Peer Management Consultants, Ltd.
- Monet, D. G. 1992, *Astronomical CCD Observing and Reduction Techniques*, 23, 221
- Piatek, S., Pryor, C., Olszewski, E. W., et al. 2002, *AJ*, 124, 3198
- Press, W.H., Flannery B.P., Teukolsky S.A., Vetterling, W.T. 1992. *Numerical Recipes in Fortran: The Art of Scientific Computing*, Cambridge University Press, 2nd edition
- Rao, C. R. 1945, *Bulletin of the Calcutta Mathematical Society* 37, 81
- Roe, B. P. 2010. *Probability and Statistics in Experimental Physics*, Springer-Verlag, New York, 2nd edition

Stone, R. C. 1989, *AJ*, 97, 1227

Stuart, A., Ord, J. K., Arnold S. 2004. *Advanced Theory of Statistics, Volume 2A, Classical inference and the linear model*, Oxford University Press, New York

van Altena, W. F., & Auer, L. H. 1975, *Image Processing Techniques in Astronomy*, 54, 411

Astrometry for Astrophysics, William F. van Altena (ed.). Cambridge University Press

van Altena, W.F. and Fomalont, E.B. 2013. In *Astrometry for Astrophysics*, William F. van Altena (ed.). Cambridge University Press, Chapter 9

Zaccheo, T. S., Gonsalves, R. A., Ebstein, S. M., & Nisenson, P. 1995, *ApJ*, 439, L43

Winick, K. A., 1986, *J. Opt. Soc. Am. A.*, 3, 1809

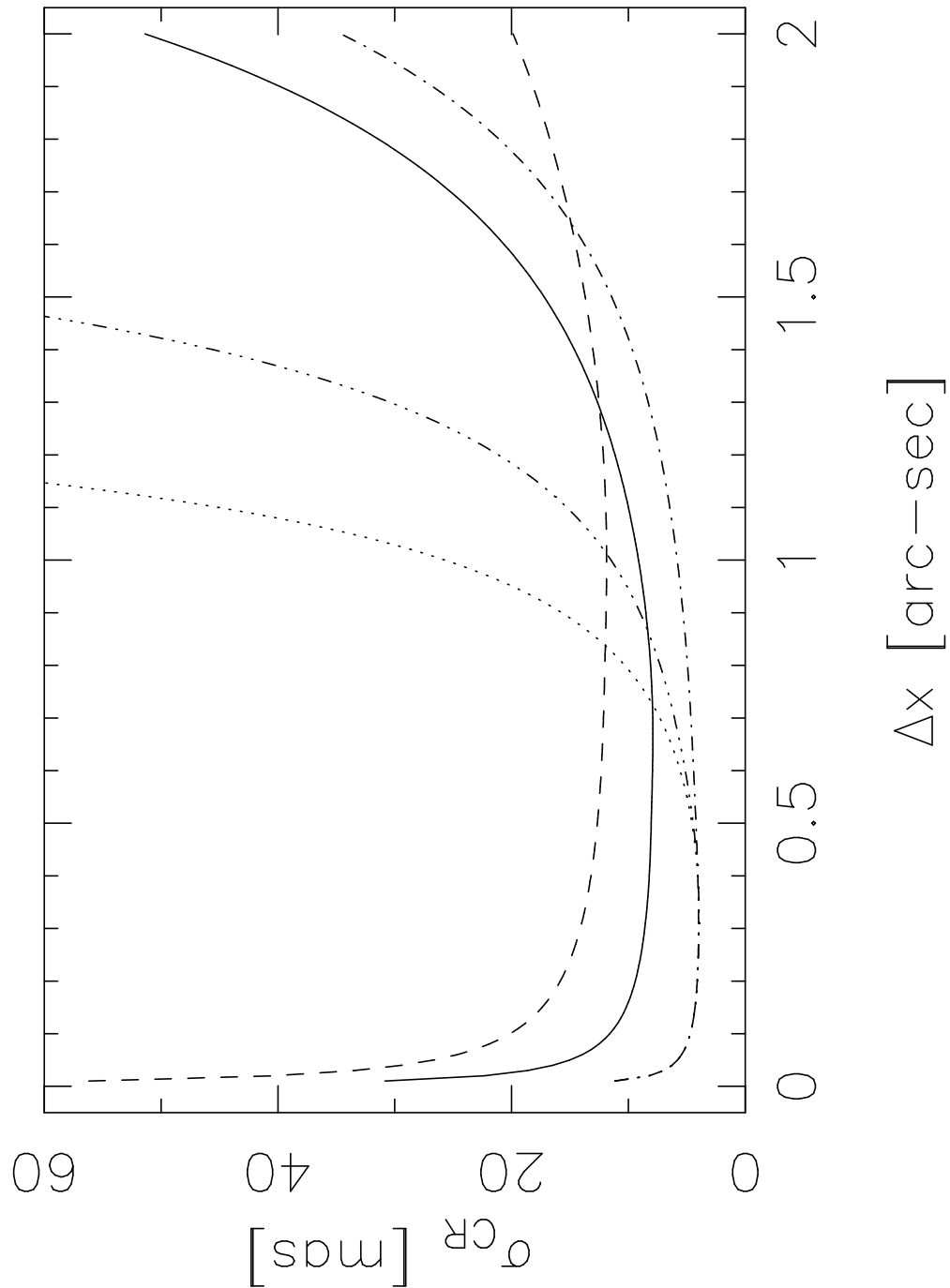


Fig. 1.— Cramér-Rao bound as given by equation (21), in milli-arcsec (mas), as a function of detector pixel size Δx in arcsec. All curves were computed for a constant background per pixel $B = 300$ ADU/pix and $F/B = 10$. The dotted, solid, and dashed lines are for a Gaussian PSF with a $FWHM$ of 0.5, 1.0, and 1.5 arcsec respectively, all centered in a given pixel of width 1.0 pixel (compare to Figure 1 in Winick (1986)). The dashed-triple dotted and dashed-dotted lines are for a $FWHM$ of 0.5 arcsec, but de-centered by 0.125 pix and 0.25 pix from the center of the pixel respectively.

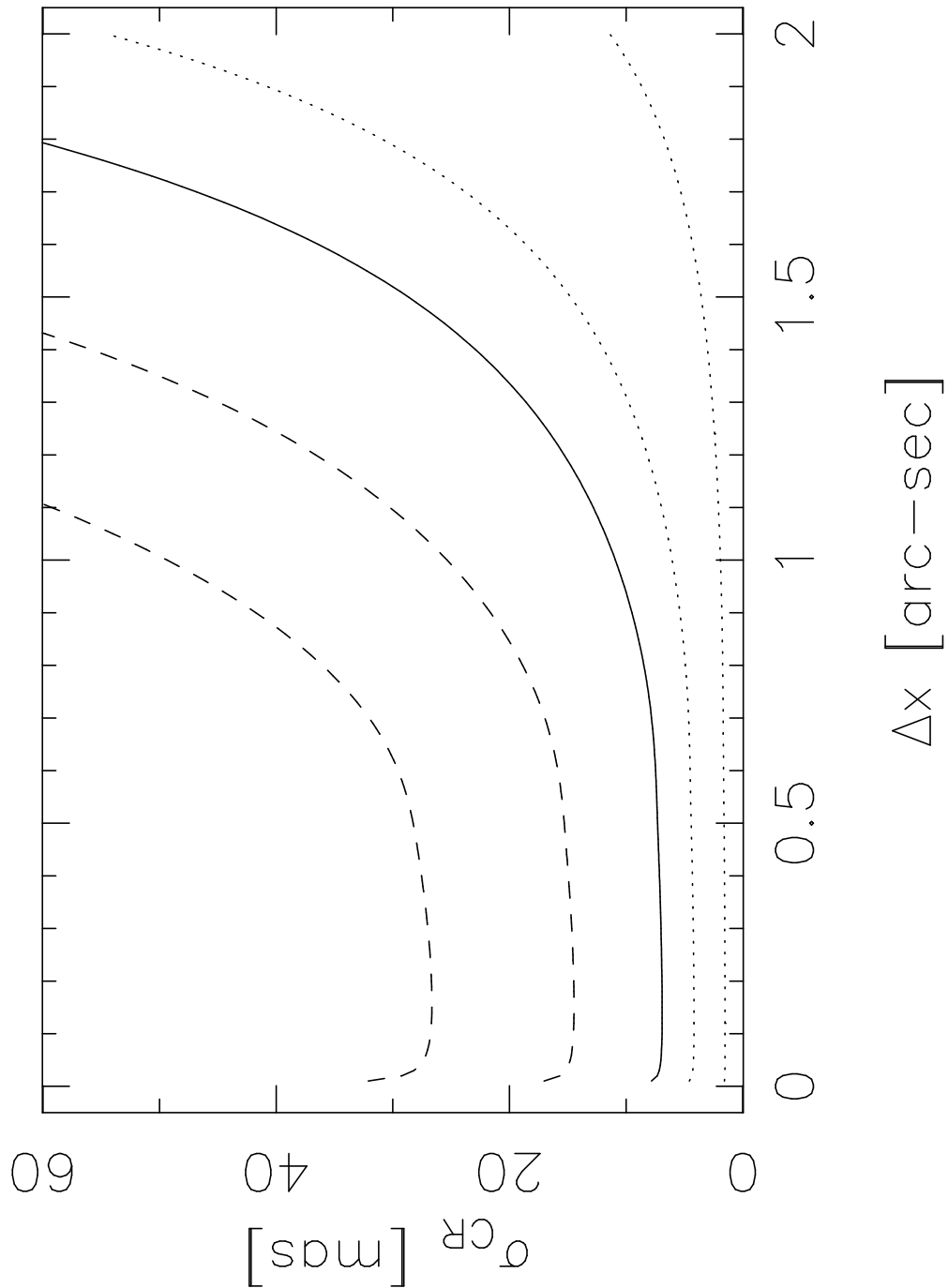


Fig. 2.— Cramér-Rao bound as given by equation (21), in milli-arcsec (mas), as a function of pixel size Δx in arcsec. All curves were computed for a background given by equation (23) with $f_s = 2000$ ADU/arcsec, $RON = 5 e^-$, $D = 0 e^-$, $G = 2 e^-/\text{ADU}$, and for a Gaussian source with $FWHM = 1$ arcsec centered on a pixel. The curves shown have different values of the flux, and hence a different S/N . From top to bottom we have $F = 1000$ ADU, $S/N \approx 20$, $F = 2000$ ADU, $S/N \approx 35$ (both dashed lines); $F = 5000$ ADU, $S/N \approx 74$ (solid line, as a reference, in this case we have $F_{\max} \approx 930$ ADU at $\Delta x = 0.2$ arcsec, see

Table 1: Cramér-Rao bound on θ as a function of pixel offset for a source with $FWHM = 0.5$ arcsec observed with two detectors of pixel size indicated by the Δx value. Other parameters are those of Fig. 1.

| Δx | Pixel offset | σ_{CR} |
|------------|--------------|----------------------|
| arcsec | pix | mas |
| 0.5 | 0.0 | 4.57 |
| 0.5 | 0.125 | 4.46 |
| 0.5 | 0.250 | 4.22 |
| 0.7 | 0.0 | 7.31 |
| 0.7 | 0.125 | 6.06 |
| 0.7 | 0.250 | 4.65 |
| 0.9 | 0.0 | 15.70 |
| 0.9 | 0.125 | 9.00 |
| 0.9 | 0.250 | 5.33 |

Table 2: Small-pixel approximation and exact Cramér-Rao bound on some limiting cases.

| Δx | $FWHM$ | F | F_{\max} | f_s | S/N^a | Exact ^b | Approx ^c |
|------------|--------|--------|------------|-------|---------|--------------------|----------------------|
| arcsec | arcsec | ADU | ADU | ADU | | mas | mas |
| 0.2 | 1.0 | 1 000 | ~186 | 2 000 | ~20 | 27 | 24 |
| 0.2 | 1.0 | 50 000 | ~ 9 308 | 2 000 | ~300 | 1.5 | 1.4 |
| 0.2 | 1.0 | 50 000 | ~ 9 308 | 500 | ~305 | 1.4 | 1.4 |
| 0.1 | 0.5 | 50 000 | ~ 9 308 | 4 000 | ~300 | 0.76 | 0.67 |
| 0.1 | 0.5 | 1 000 | ~ 186 | 4 000 | ~20 | 13 | 12 |
| 0.1 | 0.5 | 5 000 | ~ 1 024 | 4 000 | ~78 | 3.5 | 2.4/2.1 ^d |
| 0.2 | 1.0 | 5 000 | ~ 1 024 | 2 000 | ~78 | 6.9 | 4.8/4.3 ^d |

^aAs computed from equation 28 with $RON = 5 e^-$, $G = 2 e^-/ADU$, and the tabular value for Δx and f_s .

^b“Exact” Cramér-Rao bound computed from equation 21.

^cSmall-pixel approximation Cramér-Rao bound computed from equation 45, depending on if S/N is large or small.

^dThe first value is for the case of a weak source, the second for a strong source, both from equation 45.

Table 3: Comparison of the standard deviation on position σ_{x_c} from the ML and LS methods and the Cramér-Rao bound, σ_{CR} , as a function of (total) Flux.

| | | | Method: | ML | LS | WLS | Cramér-Rao |
|--------|------------------|------------|---------|---------------------|---------------------|---------------------|----------------------|
| F | F_{max} | S/N | | σ_{x_c} | σ_{x_c} | σ_{x_c} | σ_{CR} |
| ADU | ADU | | | pix | pix | pix | pix |
| 30,080 | 5600 | ~ 230 | | 0.0101 ± 0.0005 | 0.0116 ± 0.0006 | 0.0103 ± 0.0005 | 0.010 |
| 10,002 | 1862 | ~ 120 | | 0.0215 ± 0.0010 | 0.0227 ± 0.0010 | 0.0215 ± 0.0010 | 0.020 |
| 3,222 | 600 | ~ 55 | | 0.0429 ± 0.0019 | 0.0437 ± 0.0020 | 0.0431 ± 0.0019 | 0.045 |
| 1,612 | 300 | ~ 32 | | 0.080 ± 0.003 | 0.081 ± 0.004 | 0.080 ± 0.003 | 0.079 |
| 540 | 100 | ~ 12 | | 0.212 ± 0.010 | 0.212 ± 0.010 | 0.212 ± 0.010 | 0.209 |
| 268 | 50 | ~ 6 | | 0.423 ± 0.020 | 0.423 ± 0.020 | 0.423 ± 0.020 | 0.406 |

^aThe 1σ uncertainties in the derived standard deviation were computed from the variance of the variance, $Var(\sigma_{x_c}^2)$, as given by equation (3.44) in Roe (2010). It is easy to show that the uncertainty in the standard deviation would be then given by $\sqrt{Var(\sigma_{x_c}^2)}/2\sigma_{x_c}$.

Table 4. Comparison of the best 2-d digital centering algorithms (from Stone (1989)) and the Cramér-Rao bound as a function of (total) Flux.

| F ADU | <i>FWHM</i> =1 arcsec, <i>B</i> =1 ADU/arcsec | | <i>FWHM</i> =4 arcsec, <i>B</i> =1 ADU/arcsec | | <i>FWHM</i> =1 arcsec, <i>B</i> =1000 ADU/arcsec | | <i>FWHM</i> =4 arcsec, <i>B</i> =1000 ADU/arcsec | |
|----------|---|-------------------------|---|-------------------------|--|-------------------------|--|-------------------------|
| | $\Delta x = 0.125$ arcsec | | $\Delta x = 0.5$ arcsec | | $\Delta x = 0.125$ arcsec | | $\Delta x = 0.5$ arcsec | |
| | σ_{St} arcsec | σ_{CR} arcsec | σ_{St} arcsec | σ_{CR} arcsec | σ_{St} arcsec | σ_{CR} arcsec | σ_{St} arcsec | σ_{CR} arcsec |
| 100 | 0.052 | 0.047 | 0.4 | 0.2 | — | 0.24 | — | 1.9 |
| 1,000 | 0.015 | 0.014 | 0.07 | 0.055 | 0.04 | 0.029 | — | 0.20 |
| 10,000 | 0.042 ^a | 0.043 | 0.02 | 0.017 | 0.006 | 0.0053 | 0.07 ^c | 0.027 |
| 100,000 | 0.0012 ^a | 0.0014 | 0.005 ^a | 0.0054 | 0.0015 ^b | 0.0014 | 0.009 ^c | 0.0060 |

^aMoment solution.

^bFar from moment solution, as expected since *B* is large.

^cNo moment solution found.

Note. — All Cramér-Rao estimates used $G = 1 \text{ e}^-/\text{ADU}$ and $RON = 0 \text{ e}^-$.